# Kriging and Local Polynomial Methods for Blending Satellite-Derived and Gauge Precipitation Estimates to Support Hydrologic Early Warning Systems

Andrew Verdin, Chris Funk, Balaji Rajagopalan, and William Kleiber

*Abstract*—Robust estimates of precipitation in space and time are important for efficient natural resource management and for mitigating natural hazards. This is particularly true in regions with developing infrastructure and regions that are frequently exposed to extreme events. Gauge observations of rainfall are sparse but capture the precipitation process with high fidelity. Due to its high resolution and complete spatial coverage, satellite-derived rainfall data are an attractive alternative in data-sparse regions and are often used to support hydrometeorological early warning systems. Satellite-derived precipitation data, however, tend to underrepresent extreme precipitation events. Thus, it is often desirable to blend spatially extensive satellite-derived rainfall estimates with high-fidelity rain gauge observations to obtain more accurate precipitation estimates. In this research, we use two different methods, namely, ordinary kriging and $k$-nearest neighbor local polynomials, to blend rain gauge observations with the Climate Hazards Group Infrared Precipitation satellite-derived precipitation estimates in data-sparse Central America and Colombia. The utility of these methods in producing blended precipitation estimates at pentadal (five-day) and monthly time scales is demonstrated. We find that these blending methods significantly improve the satellite-derived estimates and are competitive in their ability to capture extreme precipitation.

*Index Terms*—Blending data, hydrologic early warning systems, local polynomials, ordinary kriging, rainfall estimation.

## I. INTRODUCTION

**D**ROUGHT and flood management practices require accurate estimates of precipitation in space and time. Observations from properly sited, calibrated, and maintained rain gauges are the most reliable source of information as they are direct measurements of the physical process. However, in regions of complex terrain, rain gauge data are often sparse, clustered in valleys or populated regions, and can be of poor temporal consistency. In mountainous areas, the spatial extent of extreme precipitation events tends to be underrepresented due to complications associated with the regular upkeep and data retrieval from high-elevation weather stations. In addition, mountains tend to receive more precipitation than valleys, particularly in tropical regions, which is due largely to the effects orography has on precipitation [46]. Satellite-derived rainfall data are an attractive alternative in such regions and are widely used, largely due to their ability to provide good spatial coverage. However, these estimates provide areal averages and tend to underestimate the magnitude of extreme precipitation events [2]. Other issues with satellite-derived precipitation estimates include their dependence on retrieval algorithms and the indirect relationship between satellite remote sensing measurements and precipitation intensities, which can lead to numerically inaccurate precipitation estimates [2], [12], [48]. To take advantage of the strengths of both data sources, it seems best to blend satellite-derived rainfall data of extensive spatial coverage with rain gauge observations of high fidelity.

Much of the research in this field involves deriving precipitation estimates from satellite measurements of microwave, infrared, and other signals. The Climate Prediction Center morphing method [22] produces half-hourly global precipitation estimates derived from passive microwave data. The One-Degree Daily [20] technique produces daily global precipitation estimates derived from the Threshold-Matched Precipitation Index for tropical and subtropical global regions $(40° \text{ N} - 40° \text{ S})$. The Precipitation Estimation from Remotely Sensed Information using Artificial Neural Networks [40] produces half-hourly global precipitation estimates derived from geosynchronous satellite long-wave infrared imagery and is automatically updated by incorporating the instantaneous rain-rate estimates from the Tropical Rainfall Measuring Mission [25] into the network parameter calibration process. The TRMM Multi-satellite Precipitation Analysis (TMPA) [21] produces 3-hourly global precipitation estimates derived from a calibrated combination of passive microwave precipitation estimates and infrared precipitation estimates. The TMPA also provides a delayed product (TMPA 3B42V6) that incorporates rain gauge data, effectively improving the analysis.

The products described above are produced in near real time, thus generally cannot incorporate rain gauge measurements.

A. Verdin is with the Department of Civil, Environmental, and Architectural Engineering, University of Colorado, Boulder, CO 80309 USA (e-mail: verdina@colorado.edu).

C. Funk is with the U.S. Geological Survey, Earth Resources Observation and Science Center, Sioux Falls, SD 57198 USA and also with the Department of Climate Hazards Group, Geography, University of California, Santa Barbara, CA 93106 USA.

B. Rajagopalan is with the Department of Civil, Environmental, and Architectural Engineering, University of Colorado, Boulder, CO 80309 USA, and also with the Cooperative Institute for Research in Environmental Sciences, University of Colorado, Boulder, CO 80309 USA.

W. Kleiber is with the Applied Mathematics Department, University of Colorado, Boulder, CO 80309 USA.

One of the more widely used products that incorporate rain gauge measurements is the CPC Merged Analysis of Precipitation (CMAP) [48], which covers the period from 1979 through 2012. CMAP linearly combines satellite-derived estimates (based on infrared, microwave scattering, and microwave emission methods) with output from the NCEP/NCAR Reanalysis project [23] through the maximum-likelihood estimation method. The Global Precipitation Climatology Project [1] provides global monthly precipitation analyses, also beginning in 1979, produced by merging interpolated rain gauge data provided by the Global Precipitation Climatology Center. The multisatellite estimate, which is derived from microwave and infrared radiation sensors, is bias corrected with respect to the gauge analysis and then combined with the gauge analysis via inverse-error-variance weighting.

It is known that satellite estimates can have substantial biases [2], [12], [48], often underestimating heavy rainfall amounts. Many products address this issue by combining near-real-time satellite-derived estimates with gauge-based analyses. Xie and Xiong [49] offer an approach where, first, the probability density function of the satellite data is matched with that of the gauge data and, then, an optimal interpolation technique is implemented to combine the bias-corrected satellite estimates with the gauge data. Lin and Wang [28] offer an approach to merge multiple bias-corrected satellite precipitation estimates, quantifying and removing the bias by comparison to the respective rain gauge observations.

Specific to this research, recent South American rainfall estimation work has focused on improving real-time satellite-derived precipitation estimates using robust bias correction measures. Vila *et al.* [45] developed a stepwise method for merging daily TMPA real-time (version 3B42RT) output with site-specific data for the South American continent. Two bias correction schemes are implemented: one that uses the ratio of observed and estimated rainfall and another that uses the difference. The final estimate is a weighted combination of the two schemes that minimize error and bias and was shown to have better performance than the TMPA 3B42V6 product. Rozante *et al.* [39] provide a blending technique known as MERGE that uses the Barnes objective analysis method to interpolate and combine TRMM satellite estimates with rain gauge data. The MERGE algorithm provides a quick and efficient technique for combining satellite and surface observations, specifically in regions with sparsely distributed gauge observations.

In this paper, we examine alternative approaches to blending satellite-derived precipitation estimates with rain gauge measurements, similar to the work of Vila *et al.* [45] and Rozante *et al.* [39]. The methods explored here utilize two sources of regional climate information: kriging, which takes advantage of the spatial variogram to define optimal interpolation weights, and $k$-nearest neighbor local polynomials, which uses generalized cross-validation (GCV) to optimize local fits to location and elevation surfaces. It should be noted that there have been numerous powerful extensions to the ordinary kriging model used in this research, including universal kriging, kriging with external drift, and regression kriging; greater detail may be found in standard textbooks on geostatistics [7]. The
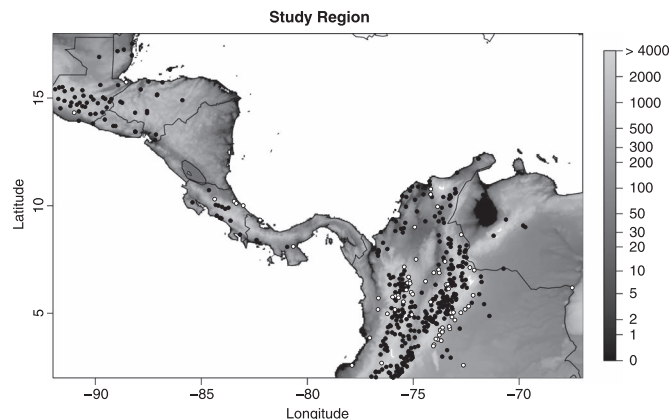


Fig. 1. Study region geography, z-scale is elevation (meters). Gauge observation locations are shown in black; locations of extreme monthly precipitation for July 2009 are in white.

research presented here is application based, with emphasis on simplicity. We aim to show that a generic ordinary kriging model, conditioned on satellite estimation error, can be as powerful as local regression. The simplicity of ordinary kriging makes it a useful tool for use across all disciplines.

The study region and data are described in the following section, followed by a description of the blending methodology, in-depth descriptions of the kriging and local polynomials frameworks, and finally, the results and discussion sections.

## II. STUDY REGION AND DATA

### A. Study Region

The study region for this research is equivalent to that in the work of Verdin *et al.* [44], which covers a Central and South American region, specifically Guatemala, Belize, El Salvador, Honduras, Nicaragua, Costa Rica, Panama, Colombia, and northwestern Venezuela (see Fig. 1). The dry season in the region extends from December through early May, and the effects of both Pacific and Atlantic tropical weather systems are felt during the wet season that extends from mid-May through November. A major contributor to the prolonged wet season is the intertropical convergence zone (ITCZ), which is an asymmetric band of convection that encircles the globe. The position of the ITCZ is nonstationary due to the seasonal shift of the trade winds.

Another cause for intense spatial variability of rainfall within the study region is its complex geography. Elevation of this area ranges from sea level to over 4000 m (as shown in Fig. 1) with numerous mountain ranges spanning Central America, Colombia, and Venezuela. Costa Rica and Guatemala have steep elevation gradients, making them vulnerable to extreme weather spawning from both Pacific and Atlantic tropical weather systems. Coastal mountain ranges cause an abrupt rising of warm wet air. As this tropical air rises, it cools and releases moisture from the air as precipitation. This is known as orographic precipitation and is a major contributor to the variability in extreme precipitation events in the region.

*B. Data*

The data used in this research are equivalent to that of Verdin *et al.* [44]. Two precipitation data sets are utilized in this research: gauge measurements and satellite-derived estimates. Rain gauge measurements are point values that tend to be clustered in populous and lower elevation areas and sparsely scattered throughout the domain; the satellite-derived estimates are high-spatial-resolution areal averages for five-day accumulations (pentads). The satellite-derived precipitation estimate used in this research is the Climate Hazards Group Infrared Precipitation (CHIRP) [13], which is a fine-resolution ($0.05° \times 0.05°$ or approximately 5 km $\times$ 5 km) pentadal product with temporal range from the first pentad of January 1981 through the near-present. There are six pentads per month, regardless of month length. For example, the sixth pentad of October will consistently be the sum of the last six days, October 26–31. The sixth pentad of February, however, will be the sum of either three or four days, depending on leap year status. Pentads may be summed up to obtain monthly totals of precipitation. The station data are sparsely scattered throughout the region (shown in Fig. 1) and were collected from partner sources of the Climate Hazards Group (CHG) at the University of California, Santa Barbara (UCSB); quality control and pentadal-aggregation techniques similar to those in the work of Funk *et al.* [13] were implemented by the CHG to produce time-series data of the same temporal range as the available CHIRP products.

## III. PROPOSED BLENDING METHODS

Before describing the methods, we introduce some notation. Let $Y_{\text{sat}}(s)$ and $Y_{\text{obs}}(s)$ be the satellite estimates and gauge observations at some location $s$, respectively. It is confirmed that the satellite estimates are of such fine spatial resolution ($0.05° \times 0.05°$) that a maximum of only one gauge observation falls within any grid cell. We assume that the fine spatial resolution of the satellite estimates allows for a direct comparison with the gauge observations. It is acknowledged that a change of support problem is present here, which will inherently include some error, but it is beyond the scope of this research. Suppose the observation network has spatial locations $s_i$, $i = 1, \ldots, N_s$, where $N_s$ is the number of gauge locations with nonmissing data for a given pentad or month. The rain gauge measurements are assigned to the nearest grid cell of the satellite estimate, where the difference between the measurements and the estimate is considered the satellite error, i.e., $r(s_i) = Y_{\text{obs}}(s_i) - Y_{\text{sat}}(s_i)$. Easting and northing (calculated in kilometers from the Prime Meridian) are used as spatial coordinates, where $s \in R^3$ includes easting, northing, and elevation.

As previously mentioned, satellite estimates tend to underrepresent the magnitude of extremes, which have a spatial structure such that extremes for a given snapshot in time tend to be related to location and elevation. This relationship suggests that the satellite error also inherits a similar spatial structure. The basis for the two blending methods used in this research is the assumption that the satellite's estimation error has an inherent spatial structure defined by location and elevation.

The blending methods involve developing a model for the dependent variable $r(s)$ as a function of covariates: easting, northing, and elevation. Note that elevation is included as a covariate due to its direct influence on precipitation occurrence, particularly in moist and tropical regions. Thus, at any desired location, i.e., $s$, the estimated satellite error $\hat{r}(s)$ is added to the satellite estimate at that location, i.e., $Y_{\text{sat}}(s)$, to obtain the estimate of true precipitation, i.e., $\hat{Y}_{\text{obs}}(s) = Y_{\text{sat}}(s) + \hat{r}(s)$. The two spatial models used in this study, namely, *ordinary kriging* and *k-nearest neighbor local polynomials*, are described below.

*A. Kriging*

Kriging is a geostatistical approach for surface estimation where the prediction at an unsampled location is calculated as a weighted linear combination of the available data that minimizes expected squared error [9]. This is a popular method applied to a variety of hydrologic and climatological applications [3], [4], [11], [15], [18], [19], [24], [26], [41], [47]. A brief description of the method is provided below, and the reader can obtain details from the aforementioned references.

The weights for this linear combination are obtained from a variogram, which defines the spatial variability of the dependent variable. Under the assumption of weak stationarity, the variogram of a given process is defined as

$$\gamma(h) = \frac{1}{2} \text{Var}\left[ r(s_i) - r(s_j) \right] \tag{1}$$

where $h = \|s_i - s_j\|$ is the Euclidean distance between observation locations $s_i$ and $s_j$. Note that the value of $h$ has units of meters because latitude and longitude are converted into easting and northing. The empirical variogram is defined as

$$\tilde{\gamma}(h) = \frac{1}{2 |N(h)|} \sum_{(i,j) \in N(h)} |r(s_i) - r(s_j)|^2 \tag{2}$$

where $N(h)$ represents the set of observation pairs, and $|N(h)|$ represents the number of observation pairs $s_i$ and $s_j$ that fall within a tolerance of a given lag $|s_i - s_j| = h$ [10]. To this, an exponential model variogram is fitted by minimizing the errors $|\tilde{\gamma}(h) - \gamma(h)|$ and has the following form:

$$\gamma(h) = C_0 + C_1 \left( 1 - \exp\left( -\frac{3|h|}{a} \right) \right), \quad |h| \geq 0 \tag{3}$$

where $C_0$ is the nugget effect, or the result of dissimilarity of sample values separated by small distances; $a$ is the effective range, or the distance at which 95% of the sill is reached; and $C_0 + C_1$ is the sill, or the maximum variogram value. The parameters of the model variogram are fitted from the binned empirical variogram, the details of which can be found in the work of Cressie [10].

The estimate of the dependent variable at any desired location $s$ is obtained as a weighted combination of all the observations as follows:

$$r(s) = \sum_{i=1}^{N_s} \lambda_i r(s_i). \tag{4}$$

The kriging weights $\lambda_i$ are obtained as a solution to the constrained optimization problem, i.e.,

$$\text{Minimize } L = E\left(r(s) - \hat{r}(s)\right)^2 \tag{5}$$

with the constraint that the weights $\lambda_i$ must sum up to 1. The standard error of the kriging predictor is the square root of the predictive mean squared error at the minimized value of $L$. The implementation can be summarized as follows.

1) Compute the empirical variogram from all pairs of observation locations.
2) Fit a theoretical variogram to the binned empirical variogram, obtaining the parameter estimates for nugget, sill, and range.
3) At any desired point $s$, obtain kriging weights via the constrained optimization problem and produce the kriged estimate.

*B.  k-Nearest Neighbor Local Polynomials*

In the context of this paper, we seek the following functional model:

$$\hat{r} = f(s) + \epsilon \tag{6}$$

where $f$ represents a mean function that is fit to a set of predictor variables $s = (\text{easting, northing, elevation})$; any number of additional variables can also be included. $\hat{r}$ is the dependent variable of interest, and $\epsilon$ is the independent normally distributed (with mean 0 and unknown variance $\sigma^2$) residual term.

In a traditional approach, $f$ is linear and estimated globally (e.g., using all the observations) leading to the familiar linear regression; in this application, it would be

$$f(s) = \beta_0 + \beta_1 X_1 + \beta_2 X_2 + \beta_3 X_3 \tag{7}$$

where $X_1$, $X_2$, and $X_3$ represent easting, northing, and elevation, respectively. The $\beta$ coefficients are estimated by minimizing the mean squared errors. Linear regression has theory that is well developed, is widely used, and can be found in any standard book [17], [37].

The global estimation of the function has several drawbacks, including 1) the assumption of a linear relationship between the independent and predictor variables over the entire range when local nonlinearities may be present, 2) the assumption of normality of input data and errors, 3) that model parameters are greatly influenced by outliers, and 4) that higher-order models require large amounts of data to fit [27], [29], [36].

A "local" or nonparametric regression method can offer an attractive alternative to alleviate the drawbacks of global function estimation. In this method, the estimate of the function at a point is influenced only by data points within a small neighborhood surrounding that point, thus providing the capability to better represent local nonlinearities in the data. Many local estimation procedures have been theorized and tested, including splines, kernel-based estimation [5], and local polynomials [29], [35]. Local polynomials are easy to understand and implement, while also offering a robust and flexible approach in estimating a variety of functions, particularly in higher dimensions. Local polynomial function estimation has been widely used in a variety of applications, such as streamflow

and salinity modeling [32], [33], streamflow forecasting [6], [16], [38], spatial estimates of precipitation [35], water quality modeling [42], and many other applications.

The methodology and the implementation steps are briefly described below; see the aforementioned references for details, particularly that by Loader [29]. In this method, a local regression of order $p$ (e.g., local polynomial) is fit at a desired point of interest, i.e., $s$, based on a neighborhood of size $k = \alpha N_s$, where $N_s$ is the total number of observations, and $\alpha$ is a fraction of observations that varies on the interval (0,1]. The $k$-nearest neighbors of $s$ are identified and weighted based on their proximity [29], and then, weighted least squares is used to fit the local polynomial or local regression of order $p$. This fitted polynomial is used to obtain an estimate of the function at the desired point $s$. The process is repeated for each point of interest. Regression theory provides the error of the estimate and, consequently, confidence and prediction intervals. Note that a local polynomial model with $\alpha = 1$, $p = 1$, and equal weights will reduce to the traditional linear regression, thus making it a general framework for function estimation.

To determine the appropriate values of $\alpha$ and $p$, objective criteria such as GCV [8] are used. The GCV function is calculated for a suite of $\alpha$ and $p$ values, and the combination with the minimum value is selected to be best. GCV can also be used to select the best subset of covariates [38]. The GCV objective function is calculated as

$$\text{GCV}(\alpha, p) = \frac{\sum_{i=1}^{N} \frac{e_i^2}{N}}{\left(1 - \frac{q}{N}\right)^2} \tag{8}$$

where $q$ refers to the number of model parameters in the current model, $N$ is the total number of observations in the current model, and $e_i$ is the residual for the $i$th data point. The denominator penalizes model complexity, thus seeking a balance between reducing errors in the numerator and complexity.

Confidence intervals of the estimate are based on estimates of standard error from the local regressions that are consistent with linear regression theory. Testing the significance of the local polynomial model with respect to alternate models such as linear regression is also done in the usual analysis of variance (ANOVA) approach; these are described in detail in [29].

Note that the kriging method also estimates the weights contributed by each observation point to the functional estimate at the desired point. However, the weights in kriging are obtained based on the fitted theoretical variogram, whereas in the local polynomial estimation procedure, they are estimated in a data-driven manner. Under some conditions, kriging can be considered as equivalent to an appropriate order spline function [31]. The goodness of the theoretical variogram is the key for good estimates from kriging, which can be difficult in practice, although other estimation methods are available.

## IV. RESULTS

Both ordinary kriging and $k$-nearest neighbor local polynomials (hereafter LP) models are applied to monthly total precipitation as well as a representative wet pentad for 2009. This research focuses on 2009 due to newly available station data for Colombia provided by partner sources of the CHG at
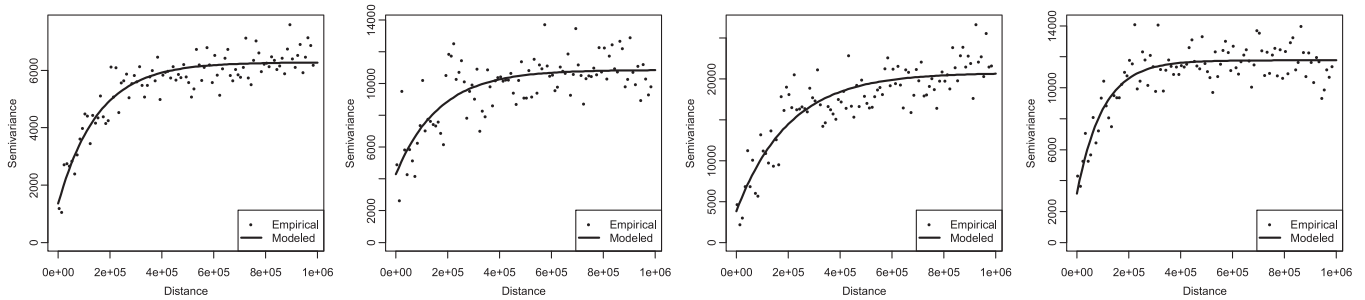
Fig. 2. Empirical (points) and theoretical (line) variograms for January, April, July, and October 2009 (from left to right, respectively).

TABLE I
$\alpha$, $p$, AND BEST SUBSET OF COVARIATES FOR LP MODEL

|  | $\alpha$ | p | k | x | y | z |
|---|---|---|---|---|---|---|
| Jan | 0.40 | 1 | 26 | * | * | - |
| Feb | 0.40 | 1 | 26 | * | * | - |
| Mar | 0.40 | 1 | 25 | * | * | - |
| Apr | 0.42 | 1 | 24 | * | * | - |
| May | 0.40 | 1 | 25 | * | * | - |
| Jun | 0.47 | 1 | 22 | * | * | - |
| Jul | 0.47 | 1 | 22 | * | * | - |
| Aug | 0.40 | 1 | 25 | * | * | - |
| Sep | 0.40 | 1 | 26 | * | * | - |
| Oct | 0.42 | 0 | 24 | * | * | - |
| Nov | 0.41 | 0 | 25 | * | * | - |
| Dec | 0.41 | 1 | 24 | * | * | - |

TABLE II
SUMMARY STATISTICS REFLECTING MODEL
PERFORMANCE FOR MONTHS IN 2009

| | Mean (mm) | RMSE (mm) | | | Bias (%) | | |
|---|---|---|---|---|---|---|---|
| | Precip | CHIRP | Krig | LP | CHIRP | Krig | LP |
| Jan | 106.1 | 76.3 | 5.2 | 53.8 | -11.1 | 0.0 | -0.5 |
| Feb | 90.2 | 77.8 | 6.3 | 54.7 | -22.5 | 0.0 | -0.9 |
| Mar | 151.7 | 99.4 | 6.2 | 63.8 | -27.1 | 0.0 | -0.8 |
| Apr | 154.9 | 91.5 | 5.4 | 61.0 | 5.2 | 0.0 | -0.5 |
| May | 183.7 | 102.3 | 6.7 | 65.5 | 17.2 | 0.0 | -0.9 |
| Jun | 206.1 | 99.1 | 6.4 | 64.6 | -0.5 | 0.0 | -0.1 |
| Jul | 263.8 | 200.1 | 9.8 | 89.7 | -49.0 | 0.0 | 0.4 |
| Aug | 169.7 | 97.8 | 6.3 | 63.5 | -0.6 | 0.0 | -0.5 |
| Sep | 124.7 | 80.7 | 6.6 | 55.7 | 12.1 | 0.0 | 0.1 |
| Oct | 196.2 | 106.9 | 7.5 | 81.8 | 16.9 | 0.0 | 0.0 |
| Nov | 159.5 | 87.9 | 5.2 | 70.2 | 8.0 | 0.0 | 0.6 |
| Dec | 80.4 | 67.6 | 4.1 | 44.1 | 25.7 | 0.0 | -0.4 |

UCSB. Analysis of results is broken into the following categories: model fitting, prediction verification, estimated maps, and performance on extreme events. Analysis was performed on several months, but we focused on January and July 2009, which are representative dry and wet months, respectively. However, in the interest of space, we show results for July 2009 and discuss the results for January 2009; figures for January can be seen in the work of Verdin [43].

Two packages (and functions) in the statistical software program R [34] provide a straightforward and user-friendly framework for implementing the kriging and LP models, respectively: fields (Krig) [14] and locfit (locfit) [30].

*A. Model Fitting*

The first step in kriging is to estimate the empirical variogram, from which a theoretical variogram is fitted, which can be seen for select months of 2009 in Fig. 2. Note that the distance $h$ is a normalized Euclidean distance with units in meters. The modeled variograms are very good at describing the spatial variability of the satellite error for a variety of months.

To summarize the LP model, Table I reports the values of $\alpha$, $p$, and the best subset of covariates as selected by GCV. The fraction of neighbors is small, and the order is generally linear (October and November yield order 0, or weighted moving average), which implies that there is great predictive skill in estimating the process locally. Moreover, note that $x$ and $y$ (easting and northing) are consistently selected as the best subset of covariates for the LP model.

The satellite error estimates are obtained from the two models at each observed location, and the CHIRP product is added to the error estimates to obtain the blended precipitation estimates. Both of these models show good skill in estimating

the observed rainfall values (see Table II for the summary statistics of all months in 2009).

As can be seen in Table II, the CHIRP estimate generally has poor representativeness of the gauge measurements, with bias values ranging from −49% to 25.7%. Similarly, its root-mean-square error (RMSE) values are quite large, with a range from 67 to 200 mm. The kriging model shows very low RMSE (all months report RMSE values lower than 10 mm) and no bias (consistently at 0.0%). However, kriging is an exact estimator; thus, no bias is expected. The LP model produces bias values with a range of less than ±1%; its RMSE values have a range of 44.1–89.7 mm.

*B. Model Validation*

To test the predictive capability of the models, cross-validations are performed. First, a leave-one-out (LOO) cross-validation is carried out, in which an observation and its covariates are dropped, the models are fitted on the rest of the data, and the dropped point is predicted using its covariates. This process is repeated for every observation, thus producing a vector of predicted values that can be validated using the vector of observations. Fig. 3 shows the scatterplots of observed and cross-validated estimates from the two models for July 2009; the scatterplot of the CHIRP product is shown for comparison. Both methods perform quite well in a cross-validated mode. Note that in July (the wet season), both the models perform much better than the CHIRP product. These findings are corroborated in Table III, which reports the summary statistics for LOO cross-validations.
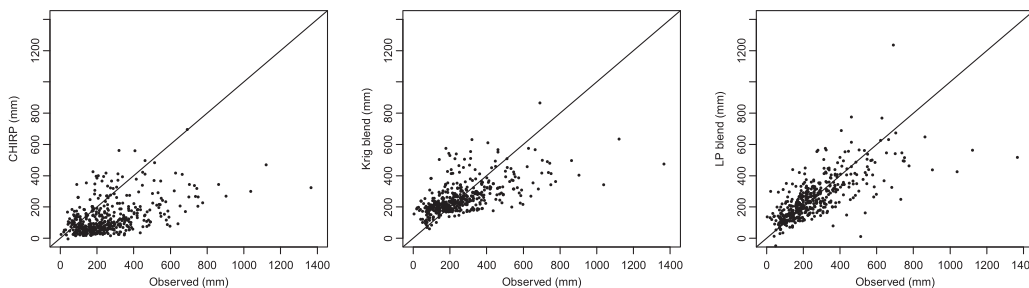
Fig. 3. Original CHIRP estimates (left) and LOO cross-validated estimates from kriging (middle) and LP (right) models for July 2009.

TABLE III
SUMMARY STATISTICS REFLECTING LOO CROSS-VALIDATION
PERFORMANCE FOR MONTHS IN 2009

| Mean (mm) | | RMSE (mm) | | | Bias (%) | | |
|-----|-----|-----|-----|-----|-----|-----|-----|
| | Precip | CHIRP | Krig | LP | CHIRP | Krig | LP |
| Jan | 106.1 | 76.3 | 68.3 | 71.3 | -11.1 | 0.2 | -0.2 |
| Feb | 90.2 | 77.8 | 62.4 | 69.5 | -22.5 | 0.8 | -0.5 |
| Mar | 151.7 | 99.4 | 77.9 | 83.0 | -27.1 | -0.1 | -0.6 |
| Apr | 154.9 | 91.5 | 74.5 | 81.3 | 5.2 | 0.1 | -0.5 |
| May | 183.7 | 102.3 | 88.1 | 82.4 | 17.2 | 0.1 | -1.4 |
| Jun | 206.1 | 99.1 | 96.3 | 90.5 | -0.5 | 0.0 | -0.2 |
| Jul | 263.8 | 200.1 | 137.0 | 128.5 | -49.0 | -0.1 | -0.5 |
| Aug | 169.7 | 97.8 | 95.4 | 92.2 | -0.6 | -0.1 | -0.6 |
| Sep | 124.7 | 80.7 | 73.9 | 71.7 | 12.1 | -0.1 | 0.3 |
| Oct | 196.2 | 106.9 | 95.7 | 93.9 | 16.9 | 0.1 | 0.0 |
| Nov | 159.5 | 87.9 | 79.6 | 80.1 | 8.0 | 0.4 | 0.7 |
| Dec | 80.4 | 67.6 | 60.7 | 58.6 | 25.7 | -0.1 | -1.8 |



Fig. 4. Prediction skill measures from drop-50% cross-validation for July 2009. Black dots correspond to estimates from original CHIRP.

The months when both spatial models show modest improvement in these measures are those when the CHIRP product has good performance. Even in predictive mode, which genuinely stresses the models, both blending methods improve upon the CHIRP product.

In the second cross-validation procedure, 25% of the observations are dropped at random and are predicted with a model fitted to the remaining data; this is repeated 500 times. Three measures are computed: RMSE, mean absolute error (MAE), and percent bias for each repetition. Drop-50% cross-validation was also performed to further stress the models, and the results are shown in Fig. 4. Note that the results from drop-25% cross-validation are similar to those from drop-50%. The CHIRP product has relatively poor performance, showing higher values for these three measures. The median values of the measures calculated from drop-50% cross-validation are comparable to those of the measures calculated from LOO cross-validation output.
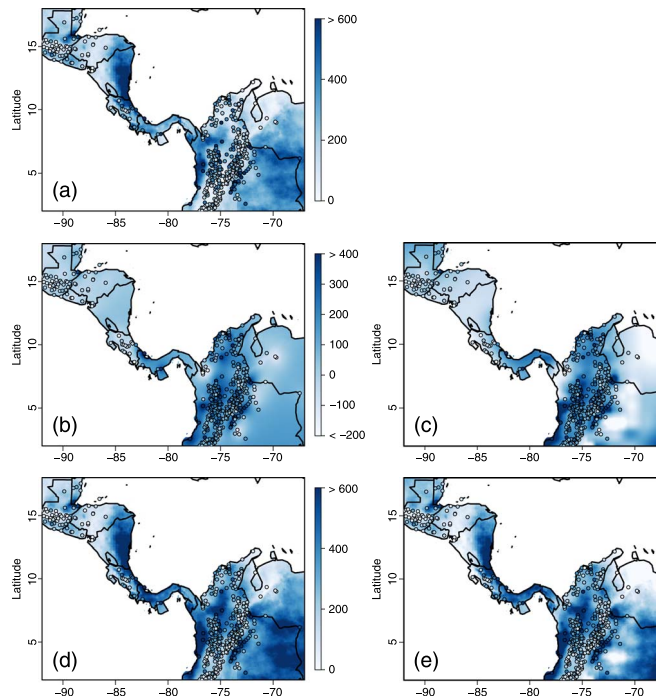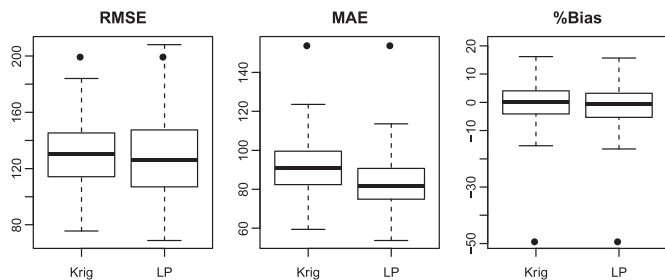


Fig. 5. (a) Original CHIRP estimates. (b) and (c) Estimated satellite error field from kriging and LP models. (d) and (e) Blended precipitation estimates from kriging and LP models for July 2009.

For both models, there is considerable decrease in RMSE and MAE for both drop-25% and -50% validation scenarios. Similarly, both models reduce the bias to nearly zero compared with the high bias in the CHIRP product. The validation performance of these blending methods for other months is similar, with varying magnitudes of improvement (figures not shown).

## C. Spatial Estimation

The models were applied to obtain blended estimates of precipitation on the satellite grid. Spatial maps of the estimates and predicted errors are shown along with the observed fields.

Spatial maps for July 2009 are shown in Fig. 5. The CHIRP product for July 2009 [see Fig. 5(a)] does a good job in capturing the spatial pattern, but fails in representing the magnitude of precipitation totals, which is due largely to July being a wet month and the inherent underestimation of satellite products during wet months. Problem areas include the Caribbean coast of Panama and the Pacific coast of Colombia, where the CHIRP product underestimates the magnitude of precipitation events. The interpolated satellite error fields from the kriging and LP
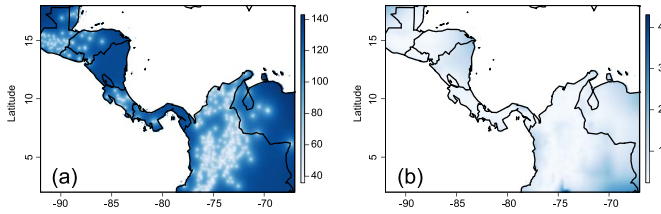
Fig. 6. Estimates of standard error of the satellite error field from (a) kriging and (b) LP models for July 2009.

models are shown in Fig. 5(b) and (c), respectively. The kriging estimates are consistent with the satellite error observations, producing a smooth and continuous residual field. The LP model also estimates values consistent with the satellite error observations, but is vulnerable to extrapolation error in data-sparse regions, such as Caribbean Venezuela. Fig. 5(d) and (e) shows the blended CHIRP products from kriging and LP, respectively. The blended estimates from the kriging model produce a spatial pattern similar to the CHIRP product, due to its tendency to estimate the expected value in regions of sparse data. Because the LP model tends to extrapolate large values of error, the blended estimates show large (and likely unwarranted) changes to the CHIRP. Despite these discrepancies, both models adjust the estimates to better match the observations in the study region.

Standard errors of both models for July 2009 are shown in Fig. 6. The standard errors of predictions from the kriging model are much lower in the regions surrounding the gauges. The LP model has much less uncertainty in its prediction process throughout the domain because it uses local functional estimation, which tends to have smaller variance [29].

The CHIRP product for January 2009 does a better job in capturing the spatial pattern and magnitude of precipitation totals when compared with that for July 2009, which is due largely to January being a dry month. Dry months in the region exhibit more widespread and spatially correlated events with low variability, which propagates to the satellite error field. Conversely, the presence of the ITCZ in wet months tends to promote highly variable and localized events, thus deteriorating the spatial correlation of the satellite error field. Regardless, model performances are comparable to those from July 2009.

### D. Performance on Extreme Events

Good estimation of extreme events is important for hydroclimatic hazard mitigation, particularly during wet months. The hazards associated with extreme events consist of floods, landslides, and agriculture overland flow, all of which are destructive to a nation's infrastructure. We define an extreme event at a gauge where monthly rainfall exceeds the 85th percentile of all observations for that month. The 85th percentile of July 2009 precipitation totals is 410 mm/month. The locations of these gauges and the majority of extreme precipitation events occur in the mountainous and coastal regions (see Fig. 1).

As can be seen in Table IV, both blending methods proposed in this research have a great impact on the performance of CHIRP with respect to extremes. These statistics are computed

### TABLE IV
SUMMARY STATISTICS OF LOO CROSS-VALIDATION BLENDING PERFORMANCE ON EXTREME EVENTS FOR JULY 2009

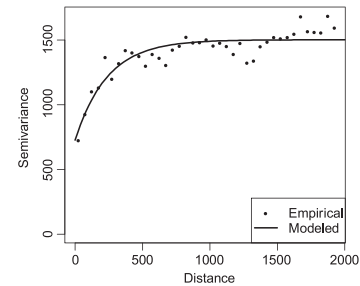|        | RMSE (mm) | MAE (mm) | Bias (%) |
|--------|-----------|----------|----------|
| CHIRP  | 386       | 344      | -58.8    |
| Krig   | 227       | 167      | -22.7    |
| LP     | 257       | 191      | -24.5    |



Fig. 7. Empirical (points) and theoretical (line) variogram for the fourth pentad of August 2009.

### TABLE V
SUMMARY STATISTICS REFLECTING MODEL PERFORMANCE FOR THE FOURTH PENTAD OF AUGUST 2009

|     | Mean (mm) | RMSE (mm) | | | Bias (%) | | |
|-----|-----------|-----------|------|------|----------|------|------|
|     | Precip    | CHIRP     | Krig | LP   | CHIRP    | Krig | LP   |
| Aug | 42.9      | 40.4      | 30.5 | 32.6 | -21.4    | 0.0  | -0.5 |

from LOO cross-validation output. Validation statistics indicate that both blending methods reduce the error and inherent bias of the CHIRP. It should be noted that models for all months in 2009 show similar skill with respect to extremes.

### E. Application to Pentad Rainfall Estimation

Here, we investigate the utility of the two blending methods to shorter temporal scales, such as pentad rainfall. This is of interest for assisting with natural hazard mitigation strategies. Accurate gridded estimates of precipitation on pentad time scales during the wet season can provide insight into the wetter regions of river basins, can be used to drive hydrologic models for modeling soil moisture, and consequently provide better risk analyses for flooding and landslides.

The fourth pentad of August 2009 will be used in this application, as it is one of the wettest pentads of 2009, yielding a maximum gauge observation of 385 mm where the CHIRP reports only 130 mm. The two blending methods as applied to the monthly precipitation described in the previous section are applied to this pentad data. Fig. 7 shows the empirical and theoretical variograms for the satellite error. During this pentad, there are multiple convective regimes that impact the spatial correlation structure; thus, there is more scatter surrounding the theoretical variogram when compared with the monthly time scale.

The CHIRP product overestimates regions of low rainfall while underestimating extremes. Table V reports the relative performance of the CHIRP, as well as the performances of the two blending methods.
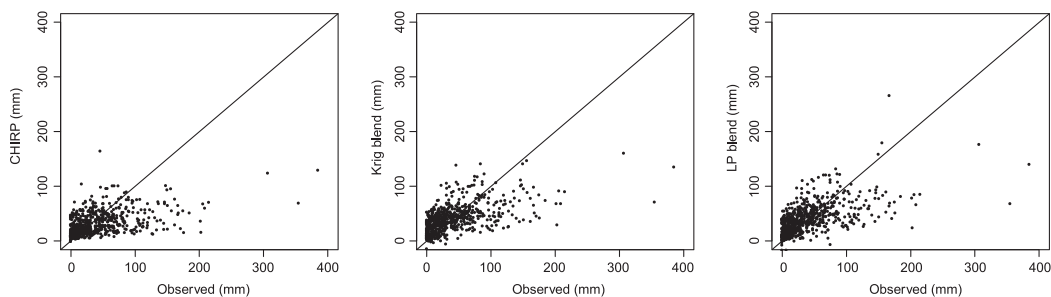
Fig. 8. Original CHIRP estimates (left) and LOO cross-validated estimates from kriging (middle) and LP (right) models for the fourth pentad of August 2009.

TABLE VI
SUMMARY STATISTICS REFLECTING LOO CROSS-VALIDATION
PERFORMANCE FOR THE FOURTH PENTAD OF AUGUST 2009

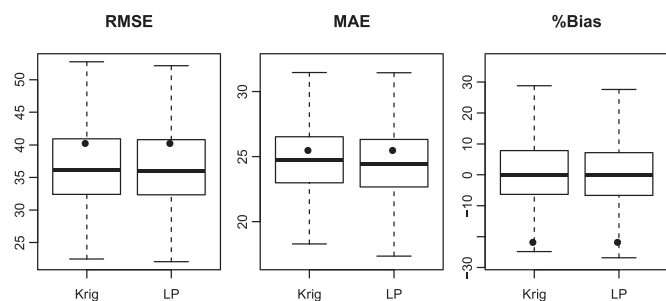| | Mean (mm) | RMSE (mm) | | | Bias (%) | | |
|---|---|---|---|---|---|---|---|
| | Precip | CHIRP | Krig | LP | CHIRP | Krig | LP |
| Aug | 42.9 | 40.4 | 36.2 | 36.5 | -21.4 | 0.2 | -0.8 |



Fig. 9. Prediction skill measures from drop-50% cross-validation for the fourth pentad of August 2009. Black dots correspond to estimates from original CHIRP.
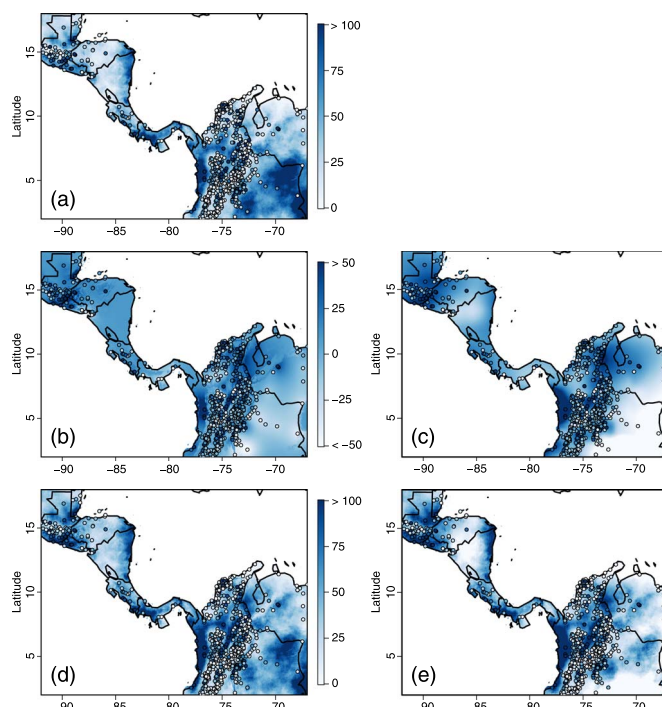


Fig. 10. (a) Original CHIRP estimates. (b) and (c) Estimated satellite error field from kriging and LP models. (d) and (e) Blended precipitation estimates from kriging and LP models for the fourth pentad of August 2009.

LOO cross-validation analyses consistent with those of the monthly totals section were carried out on this representative wet pentad. These predictions are shown as scatterplots in Fig. 8, and summary statistics are reported in Table VI.

Under LOO cross-validation stresses, the error statistics of the two blending methods are comparable to that of the CHIRP product. That being said, these blending methods eliminate the large inherent bias of the CHIRP product even in predictive mode, which is encouraging of the model's predictive skill. Both drop-25% and -50% validation techniques were applied to this pentad, yielding results consistent with the monthly totals section. Summary statistics for these validation scenarios are shown in Fig. 9. For completeness, the appropriate statistics for the CHIRP are shown as points.

Fig. 9 shows that both the kriging and LP models are robust to the predictive stresses of validation measures, consistently reducing both error and bias with respect to the CHIRP product.

The two blending methods were implemented in predictive mode to estimate the pentadal satellite error at the resolution of the CHIRP product, as in the monthly totals section. Spatial maps of the CHIRP, model estimates of the satellite error, and the blended CHIRP from kriging and LP models are shown in Fig. 10.

Problem areas include the Caribbean coast of Belize and eastern Guatemala, where the CHIRP product both over- and underestimates rain gauge measurements, respectively [see Fig. 10(a)]. Similarly, Colombia is a problem area where the CHIRP underestimates the magnitude of precipitation events on the Pacific coast and overestimates the magnitude of inland rainfall.

The kriging model estimates relatively constant values of satellite error for the Caribbean coast of Belize, although the observations are dissimilar, but captures the spatial structure of satellite error for Colombia [see Fig. 10(b)]. The LP model produces a smooth spatial map of estimated satellite error, consistent with the point values. This model captures both positive (Belize, Colombia) and negative (Colombia) satellite errors and better represents the sign and magnitude of predicted errors along the Pacific coast of Colombia [see Fig. 10(c)]. However, there is obvious extrapolation error coupled with edge effects in the southeastern corner of the study region.
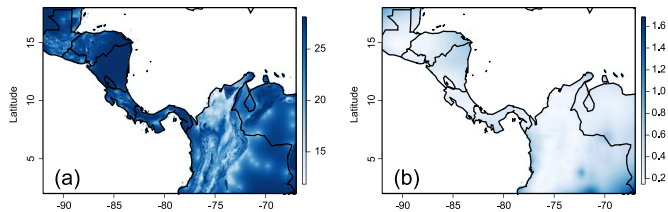
Fig. 11. Estimates of standard error of the satellite error field from (a) kriging and (b) LP models for the fourth pentad of August 2009.

TABLE VII
SUMMARY STATISTICS OF LOO CROSS-VALIDATION BLENDING
PERFORMANCE ON EXTREME EVENTS FOR THE
FOURTH PENTAD OF AUGUST 2009

|       | RMSE (mm) | MAE (mm) | Bias (%) |
|-------|-----------|----------|----------|
| CHIRP | 91        | 77       | -60.9    |
| Krig  | 78        | 63       | -48.2    |
| LP    | 77        | 61       | -44.1    |

Fig. 10(d) and (e) shows the blended estimates from the kriging and LP models, respectively. The kriging model produces a blended product with similar spatial properties as the CHIRP due to the predictive issues previously discussed. The LP model tends to reduce or increase precipitation consistent with the problem regions. However, the extrapolation and edge effects seen in mainland Colombia [see Fig. 10(c)] cause the blended product to underestimate where the CHIRP previously overestimated. Fig. 11 shows the standard error of predictions for the kriging and LP models, which are similar in spatial pattern but much smaller in magnitude to those for monthly totals.

To test the ability of these two blending methods in capturing extreme precipitation, as before we define an extreme event at a gauge where rainfall exceeds the 85th percentile of all observations for the pentad, in this case, 78 mm/pentad. The locations of these gauges and the majority of extreme precipitation events occur in the mountainous and coastal regions (consistent with Fig. 1).

Table VII summarizes how the two blending methods improve the performance of the satellite estimate with respect to extremes. These statistics are computed from LOO cross-validation output.

As seen in Table VII, the two blending methods proposed in this research are portable from monthly to pentadal scales. Both have positive impacts on the performance of the CHIRP with respect to extremes. Validation statistics show that blending reduces the error and inherent bias of the CHIRP. In light of these results, implementing these blending methods is encouraged to produce a more accurate gridded time series of precipitation.

## V. SUMMARY AND CONCLUSION

Satellite-derived estimates of precipitation are becoming widely available and in near real time, which are significant assets particularly for data-sparse regions. While these estimates provide a window into the spatial distribution and extent of precipitation, they tend to underestimate extreme precipitation events. Rain gauge observations are generally the most reliable method for capturing the magnitude of precipitation events, but

can be sparse in their spatial coverage, particularly in mountainous regions. Thus, there is a clear need to blend information from these two sources to provide robust estimates of the underlying precipitation field and its uncertainty. To this end, we offered two blending methods, namely, ordinary kriging and $k$-nearest neighbor local polynomials, and demonstrated their capabilities by applying them to precipitation data from the mountainous regions of Central America and Colombia.

In these methods, the difference between gauge observations and the nearest satellite grid cell is calculated; the two methods are applied to this "satellite error" process. Thus, at any desired location, the satellite error is estimated from the models and added to the satellite-derived product to obtain the blended precipitation estimate.

We found that both methods substantially improve the satellite-derived products, particularly during the wet season when the satellite-derived values consistently underestimate extreme precipitation events. The models were also shown to perform very well in drop-25% and drop-50% cross-validation mode. The error statistics and inherent bias are generally much lower when compared with the satellite estimates. The kriging model, however, tends to predict the expected value of the modeled process in data-sparse regions. This shortcoming causes the blended estimate to have spatial properties similar to the satellite-derived estimates. It follows that this model is useful in regions with a well-distributed network of gauges, or where isotropic spatial variability is a reasonable assumption and no change in data-sparse regions is acceptable. The LP model captures the spatial variability very well, supported by local function estimation. Furthermore, the blended estimates from the LP model incorporate the precipitation magnitudes of rain gauge observations in a smooth function. However, the LP model is much more sensitive to extrapolation and edge effects than the kriging model. Therefore, the LP model is most useful for smaller domains with great local nonlinearities in precipitation, such as mountainous regions. To exploit the strengths of both models, one could estimate the local error trend with the LP model and interpolate via kriging.

What should be emphasized in this paper is that the ability of the ordinary kriging model to withstand the stresses of cross-validation is comparable to that of the $k$-nearest neighbor local polynomials model, particularly in such a large domain. The satellite-derived product's error field is coherent and systematic such that local regression adds a minimal advantage to this methodology. The inclusion of the satellite information provides a sturdy backbone for an ordinary kriging model to produce results on par with a local regression model. This is encouraging in that scientists with limited statistical background can apply the methodology simply and swiftly. With the tools provided in this study, it is possible to retroactively improve satellite-derived estimates of precipitation, producing a robust gridded time series of precipitation over any period record, which is very useful for natural hazard mitigation and management.

Since the satellite errors are spatially modeled, both satellite and gauge precipitation data sets are required for blending. The main assumption of these two proposed methods is that the CHIRP products are unbiased estimators of the true underlying

precipitation field and that only the satellite errors need to be spatially modeled. It has been shown in this paper that CHIRP estimates are indeed biased, to such a degree that it is necessary to acknowledge this bias in the blending process. A hierarchical approach seems appropriate, where the observed precipitation is modeled as a function of CHIRP and other covariates, and the residuals from this first level are spatially modeled [44]. This addresses both issues previously described. Hierarchical modeling can be performed in a Bayesian framework, providing a posterior distribution of the parameters and subsequently that of the precipitation process at any desired location [44]. Consequently, the entire uncertainty of the parameters and estimates are easily obtained. Another extension to this approach would include the use of the entire time series of precipitation at each gauged location. In this, the first level of hierarchy previously mentioned is fitted as a generalized linear model to the satellite estimates over the entire time period at each location, and the parameters and residuals of this are spatially modeled separately [43]. Any number of covariates, including climate drivers, seasonal totals, or lagged seasonal totals, may be easily incorporated. This simple extension can enable short-term forecasting that will be of great use to decision makers and resource managers.

## REFERENCES

[1] R. F. Adler *et al.*, "The version-2 Global Precipitation Climatology Project (GPCP) monthly precipitation analysis (1979-present)," *J. Hydrometerol.*, vol. 4, no. 6, pp. 1147–1167, Dec. 2003.

[2] A. AghaKouchak, A. Behrangi, S. Sorooshian, K. Hsu, and E. Amitai, "Evaluation of satellite-retrieved extreme precipitation rates across the central United States," *J. Geophys. Res.*, vol. 116, no. D2, pp. 1–11, Jan. 2011.

[3] Z. K. Bargaoui and A. Chebbi, "Comparison of two kriging interpolation methods applied to spatiotemporal rainfall," *J. Hydrol.*, vol. 365, no. 1, pp. 56–73, Feb. 2009.

[4] Biau *et al.*, "Estimation of precipitation by kriging in the EOF space of the sea level pressure field," *J. Climate*, vol. 12, no. 4, pp. 1070–1085, Apr. 1999.

[5] A. W. Bowman and A. Azzalini, *Applied Smoothing Techniques for Data Analysis: The Kernel Approach With S-Plus Illustrations.* Oxford, U.K.: Oxford Univ. Press, 1997.

[6] C. Bracken, C. B. Rajagopalan, and J. Prairie, "A multisite seasonal ensemble streamflow forecasting technique," *Water Resources Res.*, vol. 46, no. 3, pp. 1–12, 2010.

[7] J. P. Chilés and P. Delfiner, *Geostatistics: Modeling Spatial Uncertainty.* New York, NY, USA: Wiley, 1999.

[8] P. Craven and G. Wahba, "Smoothing noisy data with spline functions," *Numerische Math.*, vol. 31, no. 4, pp. 377–403, Dec. 1978.

[9] N. Cressie, "The origins of kriging," *Math. Geol.*, vol. 22, no. 3, pp. 239–252, Apr. 1990.

[10] N. Cressie, *Statistics for Spatial Data.* New York, NY, USA: Wiley, 1993.

[11] A. J. Desbarats, C. E. Logan, M. J. Hinton, and D. R. Sharpe, "On the kriging of water table elevations using collateral information from a digital elevation model," *J. Hydrol.*, vol. 255, no. 1, pp. 25–38, Jan. 2002.

[12] E. E. Ebert, J. E. Janowiak, and C. Kidd, "Comparison of near-real-time precipitation estimates from satellite observations and numerical models," *Bull. Amer. Meteorol. Soc.*, vol. 88 no. 1, pp. 47–64, Jan. 2007.

[13] C. Funk *et al.*, "A quasi-global precipitation time series for drought monitoring," United States Geol. Survey (USGS), Earth Resources Observ. Sci. (EROS) Data Center, Sioux Falls, SD, USA, 2014, Rep. 832.

[14] R. Furrer *et al.*, Fields: Tools for Spatial Data, R Package version 6.9.1, 2012. [Online]. Available: http://CRAN.R-project.org/package=fields

[15] D. C. Garen, G. L. Johnson, and C. L. Hanson, "Mean areal precipitation for daily hydrologic modeling in mountainous regions," *J. Amer. Water Resources Assoc.*, vol. 30, no. 3, pp. 481–491, Jun. 1994.

[16] K. Grantz, B. Rajagopalan, M. Clark, and E. Zagona, "A technique for incorporating large-scale climate information in basin-scale ensemble streamflow forecasts," *Water Resources Res.*, vol. 41, no. 10, pp. 1–13, Oct. 2005.

[17] D. R. Helsel and R. M. Hirsch, *Statistical Methods in Water Resources.* Amsterdam, The Netherlands: Elsevier, 1995.

[18] M. R. Holdaway, "Spatial modeling and interpolation of monthly temperature using kriging," *Climate Res.*, vol. 6, no. 3, pp. 215–225, Jun. 1996.

[19] G. Hudson and H. Wackernagel, "Mapping temperature using kriging with external drift: Theory and an example from Scotland," *Int. J. Climatol.*, vol. 14, no. 1, pp. 77–91, Jan./Feb. 1994.

[20] G. J. Huffman *et al.*, "Global precipitation at one-degree daily resolution from multisatellite observations," *J. Hydrometeorol.*, vol. 2, no. 1, pp. 36–50, Feb. 2001.

[21] G. J. Huffman *et al.*, "The TRMM Multisatellite Precipitation Analysis (TMPA): Quasi-global, multiyear, combined-sensor precipitation estimates at fine scales," *J. Hydrometeorol.*, vol. 8, no. 1, pp. 38–55, Feb. 2007.

[22] R. J. Joyce, J. E. Janowiak, P. A. Arkin, and P. Xie, "CMORPH: A method that produces global precipitation estimates from passive microwave and infrared data at high spatial and temporal resolution," *J. Hydrometeorol.*, vol. 5, no. 3, pp. 487–503, Jun. 2004.

[23] E. Kalnay *et al.*, "The NCEP/NCAR 40-year reanalysis project," *Bull. Amer. Meteorol. Soc.*, vol. 77, no. 3, pp. 437–471, Mar. 1996.

[24] M. Kholgi and S. M. Hosseini, "Comparison of groundwater level estimation using neuro-fuzzy and ordinary kriging," *Environ. Model. Assessment*, vol. 14, no. 6, pp. 729–737, Dec. 2009.

[25] C. Kummerow, W. Barnes, T. Kozu, J. Shiue, and J. Simpson, "The Tropical Rainfall Measuring Mission (TRMM) sensor package," *J. Atmos. Ocean. Technol.*, vol. 15, no. 3, pp. 809–817, Jun. 1998.

[26] G. Laaha, J. O. Skøien, and G. Blöschl, "Spatial prediction on river networks: Comparison of top-kriging with regional regression," *Hydrol. Process.*, vol. 28, no. 2, pp. 315–324, Jan. 2014.

[27] U. Lall, "Recent advances in nonparametric function estimation: Hydrologic applications," *Rev. Geophys.*, vol. 33, no. S2, pp. 1093–1102, Jul. 1995.

[28] A. Lin and X. L. Wang, "An algorithm for blending multiple satellite precipitation estimates with in situ precipitation measurements in Canada," *J. Geophys. Res.*, vol. 116, no. D21, pp. 1–19, Nov. 2011.

[29] C. Loader, *Local Regression and Likelihood.* New York, NY, USA: Springer-Verlag, 1999.

[30] C. Loader, Locfit: Local Regression, Likelihood and Density Estimation. R package version 1.5-1.9, 2013. [Online]. Available: http://CRAN.R-project.org/package=locfit

[31] G. Matheron, "Splines and kriging: Their formal equivalence," in *Proc. Syracuse Univ. Geol. Contrib.*, 1981, pp. 77–95.

[32] J. Prairie and B. Rajagopalan, "Statistical nonparametric model for natural salt estimation," *J. Environ. Eng.*, vol. 131, no. 1, pp. 130–138, Jan. 2005.

[33] J. Prairie, B. Rajagopalan, T. Fulp, and E. Zagona, "Modified K-NN model for stochastic streamflow simulation," *J. Hydrol. Eng.*, vol. 11, no. 4, pp. 371–378, Jul. 2006.

[34] "R: A language and environment for statistical computing," R Develop. Core Team, Vienna, Austria, 2011. [Online]. Available: http://www.R-project.org/

[35] B. Rajagopalan and U. Lall, "Locally weighted polynomial estimation of spatial precipitation," *J. Geographic Inf. Decision Anal.*, vol. 2, no. 2, pp. 44–51, Feb. 1998.

[36] B. Rajagopalan *et al.*, "Ensemble streamflow forecasting: Methods and applications," in *Advances in Water Science Methodologies*, U. Aswathanarayana, Ed. Leiden, The Netherlands: A. A. Balkema, 2005.

[37] C. R. Rao and H. Toutenburg, *Linear Models, Least Squares and Alternatives.* New York, NY, USA: Springer-Verlag, 1999.

[38] S. K. Regonda, B. Rajagopalan, M. Clark, and E. Zagona, "A multimodel ensemble forecast framework: Application to spring seasonal flows in the Gunnison River Basin," *Water Resources Res.*, vol. 42, no. 9, pp. 1–14, Sep. 2006.

[39] J. R. Rozante, D. S. Moreira, L. G. G. de Goncalves, and D. A. Vila, "Combining TRMM and surface observations of precipitation: Technique and validation over South America," *Amer. Meteorol. Soc.*, vol. 25, no. 3, pp. 885–894, Jun. 2010.

[40] S. Sorooshian *et al.*, "Evaluation of PERSIANN system satellite-based estimates of tropical rainfall," *Bull. Amer. Meteorol. Soc.*, vol. 81, no. 9, pp. 2035–2046, Sep. 2000.

[41] C. Tobin, L. Nicotina, M. B. Parlange, A. Berne, and A. Rinaldo, "Improved interpolation of meteorological forcings for hydrologic applications in a Swiss Alpine region," *J. Hydrol.*, vol. 401, no. 1/2, pp. 77–89, Apr. 2011.

[42] E. Towler, B. Rajagopalan, and R. S. Summers, "Using parametric and nonparametric methods to model total organic carbon, alkalinity, and pH after conventional surface water treatment," *Environ. Eng. Sci.*, vol. 26, no. 8, pp. 1299–1308, Aug. 2009.

[43] A. Verdin, "Statistical methods for blending satellite and ground observations to improve high-resolution precipitation estimates," M.S. thesis, Dept. Civ. Env. Arch. Engr., Univ. Colorado, Boulder, CO, USA, Dec. 2013.

[44] A. Verdin, B. Rajagopalan, W. Kleiber, and C. Funk, "A Bayesian kriging approach for blending satellite and ground precipitation observations," *Water Resources Res.*, vol. 51, no. 2, pp. 908–921, Feb. 2015.

[45] D. A. Vila L. G. G. de Goncalves, D. L. Toll, and J. R. Rozante, "Statistical evaluation of combined daily gauge observations and rainfall satellite estimates over continental South America," *J. Hydrometeorol.*, vol. 10, no. 2, pp. 533–543, Apr. 2009.

[46] J. M. Wallace and P. V. Hobbs, *Atmospheric Science: An Introductory Survey*. Waltham, MA, USA: Academic, 2006, pp. 20–21.

[47] J. Wilk *et al.*, "Estimating rainfall and water balance over the Okavango River Basin for hydrological applications," *J. Hydrol.*, vol. 331, no. 1/2, pp. 18–29, Nov. 2006.

[48] P. Xie and P. A. Arkin, "Global precipitation: A 17-year monthly analysis based on gauge observations, satellite estimates, and numerical model outputs," *Bull. Amer. Meteorol. Soc.*, vol. 78, no. 11, pp. 2539–2558, Jun. 1997.

[49] P. Xie and A. Y. Xiong, "A conceptual model for constructing high-resolution gauge-satellite merged precipitation analyses," *J. Geophys. Res.*, vol. 116, no. D21, pp. 1–14, Nov. 2011.

**Andrew Verdin** is currently working toward the Ph.D. degree in water resources engineering at the University of Colorado at Boulder, Boulder, CO, USA.

His research interests include spatial statistics, remote sensing applications, stochastic forecasting and simulation, hydrology, and Bayesian modeling. His current research is focused on space–time modeling techniques for agricultural decision support in the Pampas of Argentina.

**Chris Funk** is a Research Geographer working with the United States Geological Survey and the Geography Department, University of California, Santa Barbara, CA, USA. Since 1999, he has worked closely with the US Agency for International Development Famine Early Warning System Network. He also works closely with the U.S. Geological Survey Earth Resources Observation and Science Center and African scientists in Nairobi, Gabarone, and Niamey. His research focuses on research supporting food security, tropical rainfall analysis and prediction, hydro-climatology, and African climate change.

**Balaji Rajagopalan** received the B.Tech. degree in civil engineering from the National Institute of Technology, Kurukshetra, India; the M.Tech. degree in optimization and reliability engineering from the Indian Statistical Institute, Calcutta, India; and the Ph.D. degree from Utah State University, Logan, UT, USA, with a specialization in stochastic hydrology and hydroclimatology.

He has published over 90 journal articles in a variety of journals, including the prestigious *Science and NatureGeoscience*. His research focuses on 1) understanding the large-scale climate drivers of year-to-year and multi-decadal variability of regional hydrology (i.e., precipitation, streamflow, etc.), 2) developing ensemble hydrologic forecast and simulation tools that incorporate large-scale climate information, 3) coupling the forecasts with the water resource decision support system, and 4) understanding monsoonal climate variability and predictability. His research has proven to be of immense value in the operations, management, and planning of water resources in the semiarid river basins of Western USA, particularly the Colorado River System.

Dr. Rajagopalan was a corecipient of the Partners In Conservation Award from the Department of Interior in 2009, in recognition of his research work. He has also developed tools to quantify uncertainty in input water quality to water treatment plants. For his joint work on unraveling the mystery of Indian summer monsoon droughts that appeared in *Science* in 2006, he was a corecipient of the prestigious Norber Gerbier Mumm Award from the World Meteorological Organization in 2009. He has served on the US CLIVAR panel on Prediction, Predictability and Applications, which is one of the main bodies that helped set the United States climate research agenda. He is also the Associate Editor of *Geophysical Research Letters*, *Water Resources Research*, *Climate Research*, and the *Journal of Hydrologic Engineering*.

**William Kleiber** received the B.S. degree in mathematics (with honors and distinction) from the University of Iowa, Iowa City, IA, USA, in 2006 and the Ph.D. degree in statistics from the University of Washington, Seattle, WA, USA, in 2010.

From 2010 to 2012, he was a Postdoctoral Scientist with the National Center for Atmospheric Research in the Geophysical Statistics Program. He is currently an Assistant Professor with the Department of Applied Mathematics, University of Colorado at Boulder, Boulder, CO, USA. His research interests focus on the theoretical and methodological aspects of spatial statistics, geostatistical techniques for large data sets, stochastic weather simulation, and computer experiment calibration and validation.